On the Feasibility of a Direct Injection Probe with a Capacitively Coupled Return and Integrated Voltage Monitor

Aaron Harmon
Dept. of Electrical and Computer
Engineering – Electromagnetic
Compatibility Laboratory
Missouri University of Science
and Technology
Rolla, MO, USA
afhpq4@umsystem.edu

Daniel Szanto
Dept. of Electrical and Computer
Engineering – Electromagnetic
Compatibility Laboratory
Missouri University of Science
and Technology
Rolla, MO, USA
dpsn2x @umsystem.edu

Dr. Victor Khilkevich
Dept. of Electrical and Computer
Engineering – Electromagnetic
Compatibility Laboratory
Missouri University of Science
and Technology
Rolla, MO, USA
khilkevichv @umsystem.edu

Dr. Daryl Beetner
Dept. of Electrical and Computer
Engineering – Electromagnetic
Compatibility Laboratory
Missouri University of Science
and Technology
Rolla, MO, USA
daryl@umsystem.edu

Abstract — Characterizing the susceptibility of an IC while it is integrated within a system can be challenging. Characterization is even harder if one wants to know the waveform at the target IC pin when injecting a signal on the pin. In this work, the feasibility of a direct injection probe with a capacitively coupled return and integrated voltage monitor is proposed. This probe is advantageous because it does not need to be soldered to the test device and its ability to provide a measurement of the waveform on the target IC pin during the injection. Methods for reconstructing the pin waveform based on probe measurements are discussed. Initial results indicate that the presented probe is generally insensitive to landing position variations and can accurately provide the waveform at the target IC during an injection. Future work is focused on further validation of the presented probe.

Keywords— Conducted Susceptibility, Direct Power Injection, HPEM, Immunity, IEMI, Susceptibility

I. INTRODUCTION

The Direct Power Injection (DPI) test method outlined by IEC 62132-4 [1] is widely used to characterize the electromagnetic immunity of integrated circuits (IC) [2–6]. In this method, a continuous wave aggressor is injected into a victim circuit and the forward and reflected power is recorded such that the net power injected into the target can be calculated. Aspects of this methodology have also been realized for transient aggressors such as EFT, ESD, and pulsed RF aggressors [7–10] to characterize the immunity of a target IC.

In each of the above works the target IC was placed on a custom-made printed circuit board (PCB) for immunity characterization. Custom PCBs allow for controlled impedance traces to be run directly to the pin(s) of interest but can be costly and complicated to design especially when multiple pins on a target IC are to be characterized. Moreover, custom PCBs often do not reflect the real-world system, both in terms of the parasitics and intercomponent interaction, in which target IC exists and in many cases testing for IC susceptibility is not possible if the IC is not integrated along with many the support components that allow it to operate. An alternative to characterizing the target IC on a custom PCB is to perform an in-system immunity characterization where the

target IC remains in a system containing the target IC. This approach is not without its own set of challenges, however, as one needs a probe that can monitor both the injection into and reflection from the target IC to calculate the nodal voltage at the target IC during the characterization. Without this information, one can only characterize the target IC's immunity based upon the level of the injection into the probe which may not accurately reflect the level on the target IC, especially for transient pulses.

In [11] a probing structure that can measure the nodal voltage at the target was used to characterize the immunity of a D-Flip Flop. The probing structure was realized by soldering a 500-ohm pickup resistor between the injection line and a semi-rigid monitor cable, whose shield was connected to the return of the system. While this probing structure can work for in-system immunity characterization, its solder-in nature makes it intrusive and increases the test time required to characterize the target. Moreover, the structure's requirement of a direct current (DC) coupled return can make this probing structure infeasible for testing all pins on the target IC as the many components surrounding the target and layout limitations of the systems PCB can make this return inaccessible.

In [12] a coaxial cable was suggested to be used as a probe for performing an in-system immunity characterization. The return of this probe is capacitively coupled to the return of the system and does not require a DC-coupled return. The probe from [12] is non-invasive and can easily be moved from pin to pin on a target, which reduces test time. Further, this probe can also inject into the target IC directly or indirectly through an inline capacitance to not load the target IC with a DC impedance. While the probe from [12] has many advantages, the probe does not have an integrated voltage monitor and cannot provide the waveform at the target IC during the injection. This is a major detriment to fully characterizing the susceptibility levels of each pin.

Many passive and active probes exist to measure a target IC in-system [13, 14], but these probes only allow for measurement, not injection, nor the combination. In this work, the authors propose a direct injection probe that combines the features of the probing structure from [11] with the features of

the probe from [12]. Like the probe in [12], the proposed probe is non-invasive, can perform capacitive or direct injections, and the return of the proposed probe is capacitively coupled to the return structure of the system. However unlike the probe from [12] the proposed probe has an integrated voltage monitor, realized via a high impedance pickup resistor, that allows for a combination of the injected and reflected wave to be measured during the injection. Using this additional information, the nodal voltage at the target IC during an injection can be calculated and the target IC can be characterized via this voltage as opposed to the voltage of the source. To the author's knowledge, this is the first non-invasive in-system immunity characterization probe that can provide the waveform apparent at the target IC during the injection.

In Section II the theory of operation of the proposed probe is described and formulations to calculate the nodal voltage at the target IC are given. In Section III the probe is realized, and key design aspects are discussed. In Section IV the scattering parameters of the probe are measured and the probe's sensitivity to variations in landing position is discussed. In Section V experimental results as shown to demonstrate the feasibility of the proposed probe. Finally, in Section VI the work is concluded and a discussion on relevant topics and future work is given.

II. THEORY OF OPERATION

Fig. 1 shows a high-level schematic of the proposed probe. The probe is a three-port device with one internal node. Port one is the injection port and is directly connected to the internal node via transmission line T1. Port two is the pickup port and is connected to the internal node via transmission line T2 and a high-impedance resistor which allows the voltage of the internal node to be monitored during an injection without loading the injection line (provided that the impedance of the pickup resistor is much larger than the impedance of the target impedance including the probe parasitics). Port 3 is the victim IC port and is connected to the center conductor of the injection line via a short needle. This needle injects the signal into the victim IC and is represented by the parasitic inductance from the internal node to the port.

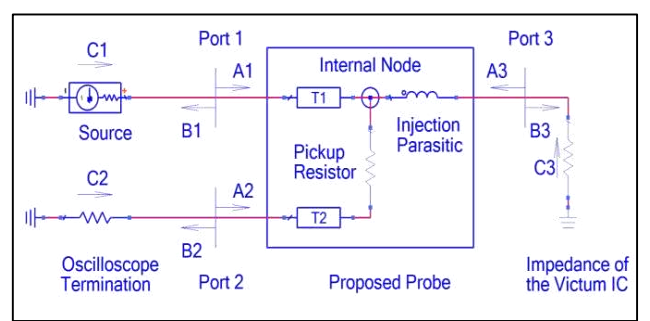


Fig. 1. High-level schematic of the proposed probe. The probe return and the victim IC returns are capacitively coupled (not shown).

The return of the probe is capacitively coupled to the return structure of the system under test (nominally the return plane of the system PCB) by the parasitic capacitance inherent between the return of the probe and the return structure of the

system. This coupling cannot be fully described by a simple lumped element schematic and hence is omitted from Fig. 1 for simplicity. The scattering parameters (S-parameters) of the probe best describe this coupling and can be obtained from 3D simulation or measurement of the probe as shown in section IV. A 3D simulation of the probe is not shown in this work in lieu of measurement data obtained in Section IV.

To illustrate how the wave amplitudes at port 3 are calculated for the proposed probe the general representation of a 3-port circuit is introduced in (1). In (1) A_N and B_N represent the transmitted and reflected wave for port N, Γ_{LN} represents the reflection coefficient of the load termination at port N, C_N represents the external stimulus incident on port N, and S_{NM} represents the S-parameters between ports N and M respectively [15]. Note that S-parameters are complex numbers and both the real and imaginary parts of the S-parameters are considered in the presented equations.

$$\begin{bmatrix} -1 & \Gamma_{L1} & 0 & 0 & 0 & 0 \\ S_{11} & -1 & S_{12} & 0 & S_{13} & 0 \\ 0 & 0 & -1 & \Gamma_{L2} & 0 & 0 \\ S_{21} & 0 & S_{22} & -1 & S_{23} & 0 \\ 0 & 0 & 0 & 0 & -1 & \Gamma_{L3} \\ S_{21} & 0 & S_{22} & 0 & S_{23} & -1 \end{bmatrix} \begin{bmatrix} A_1 \\ B_1 \\ A_2 \\ B_2 \\ A_3 \\ B_2 \end{bmatrix} = \begin{bmatrix} -C_1 \\ 0 \\ -C_2 \\ 0 \\ -C_3 \\ 0 \end{bmatrix}$$
(1)

Equation (1) can be simplified into (2) using the following conditions for the circuit in Fig. 1: the stimulus exists only at port 1, such that $C_2 = C_3 = 0$; the source and the oscilloscope are perfectly matched, resulting in $C_1 = A_1$, $A_2 = 0$, $\Gamma_{L1} = \Gamma_{L2} = 0$; because $A_2 = 0$, the quantity B_2 is equal to the voltage measured by the oscilloscope and is known.

$$\begin{bmatrix} S_{11} & -1 & S_{13} & 0 \\ S_{21} & 0 & S_{23} & 0 \\ 0 & 0 & -1 & \Gamma_{L3} \\ S_{31} & S_{33} & 0 & -1 \end{bmatrix} \begin{bmatrix} A_1 \\ B_1 \\ A_3 \\ B_2 \end{bmatrix} = \begin{bmatrix} 0 \\ B_2 \\ 0 \\ 0 \end{bmatrix}$$
 (2)

Equation (2) is then solved using the measured pickup waveform, i.e. $B_2 = V_{scope}$, and the load reflection coefficient Γ_{L3} to yield the wave amplitudes at ports 1 and 3. The quantity A_1 represents the excitation signal, and the target voltage is obtained by the sum $V_{IC} = A_3 + B_3$ The wave amplitudes can then be summed to find the nodal voltages at ports 1 (injected signal) and 3 (induced voltage). The load reflection coefficient Γ_{L3} can be obtained by the S-parameter measurement of the target in advance using a variety of methods [16, 17].

III. PROBE CONSTRUCTION

Fig. 2 shows the probe built following the schematic in Fig. 1. The input SMA connectors are connected to the internal node using two 0.96-mm diameter semi-rigid cables mounted on a 1-mm thick FR4 substrate. A 750-ohm 0402 resistor was used as the pickup resistor. The pickup resistor was soldered between the center conductors of the semi-rigid cables along with the needle. This connection is shown in Fig. 3. The pickup resistor was then wrapped in heat shrink tubing to increase the mechanical stability of the connection. The area shown in Fig. 3 is indicated by the red circle in Fig. 2.

The value of the pickup resistor does not have to be 750 ohms, however, the selected value will affect the sensitivity of the probe and loading of the target. Larger resistor values will decrease the loading of the IC but also increase the attenuation observed between the internal node and port 2, therefore decreasing the sensitivity of the probe. Conversely, a smaller resistor value will increase the sensitivity of the probe but also increase the loading.

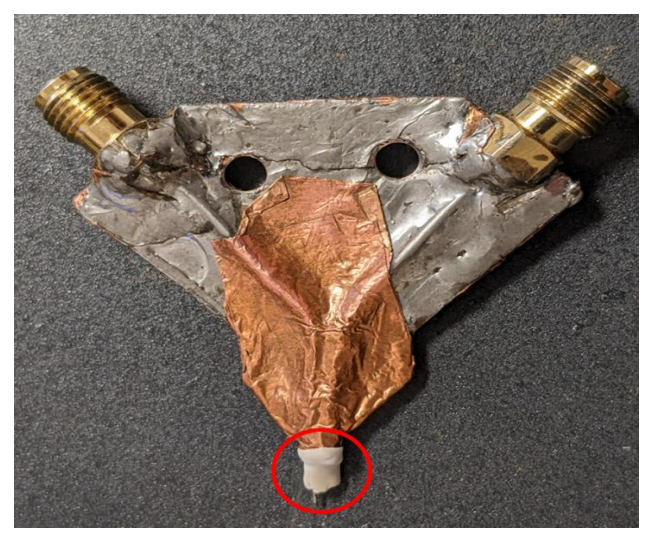


Fig. 2. Image of the realized probe. The semi-rigid cables have been soldered to the FR4 substrate and the pickup resistor mounted as shown in Fig. 3. Heat shrink tubing (white) has been added to enhance the mechanical stability of the needle. The red circle indicates the area shown in Fig. 3.

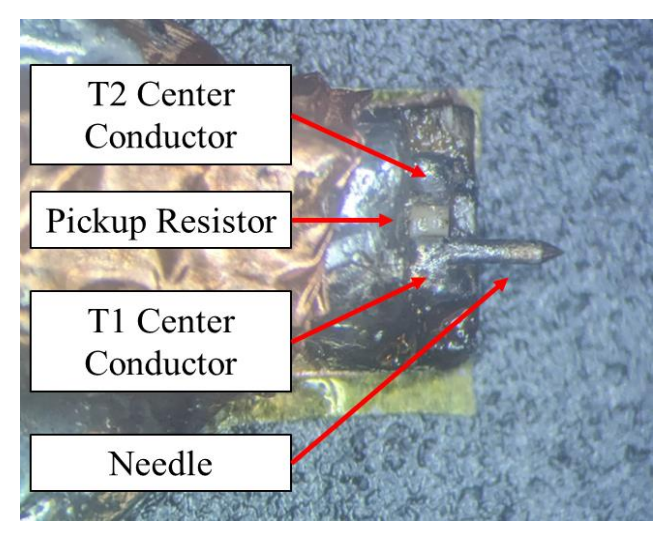


Fig. 3. Image of the pickup resistor mounting before application of the heatshrink tubing. The pickup resistor was placed between the two center conductors of semi-rigid cables along with the probing needle.

The injection needle was realized using a 1.7-mm long, 0.3-mm diameter, tin-plated copper needle. The smaller the parasitic inductance of the needle the better the probe performance. Shorter and wider needles reduce the parasitic inductance of the needle. The converse is true for longer and thinner needles. Reducing the parasitic inductance is

advantageous because doing so also reduces the insertion loss of the injection line. This may not be possible in all cases, however, such as when the victim IC has a small pin pitch and a thin needle might be needed, or when components on the PCB block direct access to the injection point and a longer needle might be needed. Factors such as the pickup resistor value and the needle properties should be considered by the designer and balanced to create a probe that is most suitable for the in-system immunity characterization they wish to perform.

IV. S-PARAMETERS OF THE REALIZED PROBE

A. S-Parameter Measurement

As shown in (2) the S-parameters of the probe are needed to calculate the induced voltage at the target pin. A characterization plate was constructed to measure the S-parameters of the probe. This plate was a 100 mm² flat copper plate with an SMA port embedded at the center as shown in Fig. 4. The probe was then affixed to a micro positioner and landed on the characterization plate such that the tip of the needle touched the center conductor of the port. The S-parameters of the probe were then measured using a calibrated N5245A PNA from 100 MHz to 17 GHz. The resulting S-parameter measurements are shown in Fig. 5 (only the terms relevant to (2) are shown).



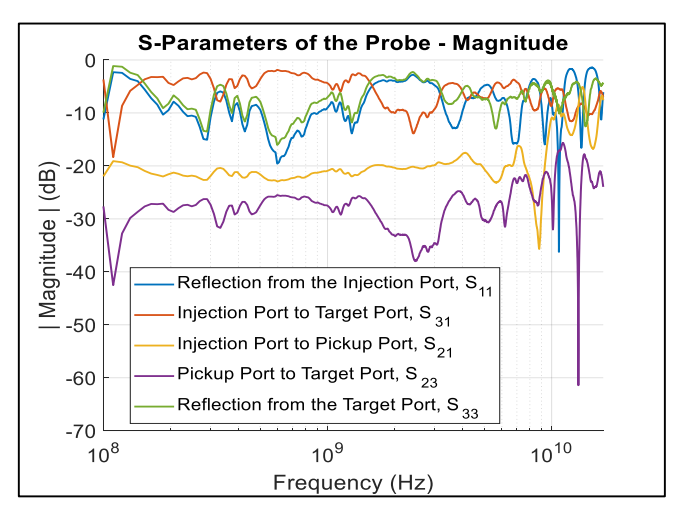


Fig. 4. (Left) The realized probe attached to a micro positioner for S-parameter measurement. (Right) A magnified image of the probe landed on the center conductor of the SMA port for S-parameter measurement.

By analyzing the measured S-parameters of the probe one can deduce the usable frequency range of the constructed probe. The main limiting factor for this probe is the presence of sharp nulls in its frequency responses, in particular in the transmission coefficient from the injection port to the target and from the target to the monitor port. These nulls can introduce error or uncertainty into the calculation due to their strong sensitivity on the probe position and similar factors. The presence of these high-frequency nulls limits the upper usable frequency range of the probe to 8 GHz. Similarly, the nulls at 110 MHz in both the S₃₁ and S₂₃ parameters will likely make the probe unusable below 200 MHz.

The insertion loss between the injection and target ports is mainly due to the discontinuity in the probe return and the parasitic inductance associated with the probing needle. A relatively low insertion loss between the injection to the target (S₃₁) at a level from -3 to -6 dB is observed in the frequency range from 200 MHz to 1.5 GHz, which determined the most usable frequency range of the probe. In applications where the loss of the injected power is not critical, the frequency range can be extended to 8-9 GHz. Less reflections were hoped for at port 1, but the observed reflection level does not overly limit the probe application, since the reflection can be relatively easily diverted from the source output by using an isolator.

Because the probe is constructed from two transmission lines and two lumped components (the pickup resistor and injection needed) one would expect the phase of the probe to resemble that of a transmission line. Indeed, the phase term of the measured s-parameters meets the expectation of a transmission line structure.



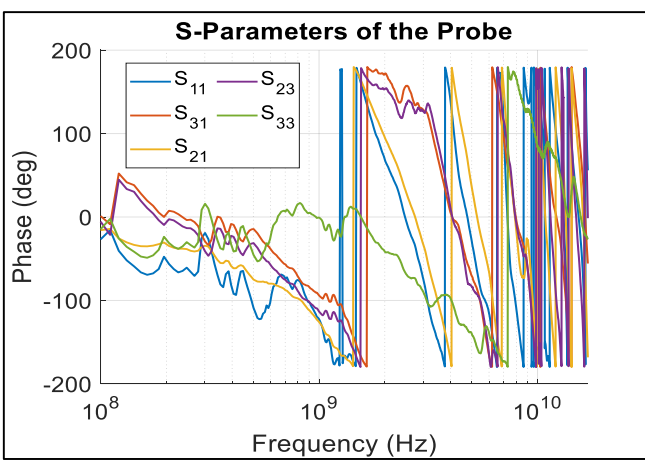


Fig. 5. The S-parameters of the probe required for (2). These parameters were measured as described in Section IV and as shown in Fig. 4. (Top) Magnitude of the measurement. (Bottom) Phase of the measurement.

The loading impedance of the probe (Z_{33}) was calculated from the measured S-parameters with ports 1 and 2 terminated by a 50 Ohm impedance. The magnitude and phase of this

impedance is shown in Fig. 6. Three distinct regions can be observed in Fig. 6. Lines of best fit were determined for these regions to give the reader an impression of the approximate loading of the probe within each region. In region 1 (100 MHz $-1.6~\rm GHz)$ the probe resembles a 100 Ohm shunt resistor. In region 2 (1.6 $-8~\rm GHz)$ the probe resembles a 0.89 pF shunt capacitor. In region 3 (8 $-17~\rm GHz)$ the probe resembles a 0.84 nH shunt inductance. Again, these values are approximations as a more complicated model would be required to fit the measured impedance curve. The development of said model is outside the scope of this work.

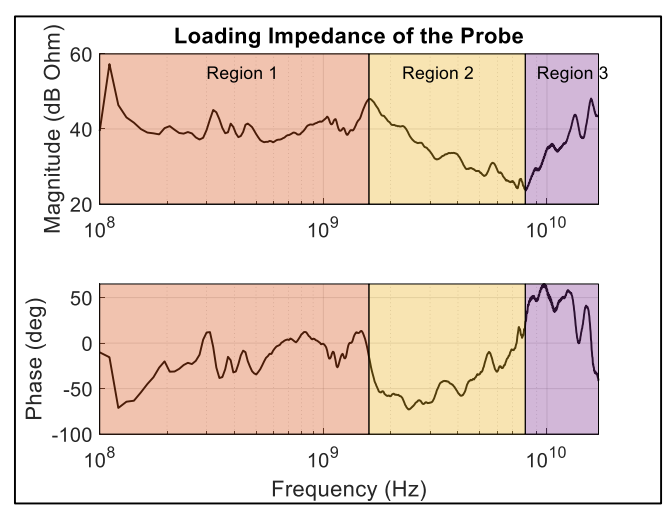


Fig. 6. Loading impedance of the probe calculated from the S-parameters during the probe characterization.

B. Sensitivity to Variations in the Landing Position

Variations in the landing position of the probe can lead to variations in the probe's S-parameters. Differences between the measured values of S-parameters used to calculate pin waveforms with (2) and their actual values at the time of injection will introduce errors in the target IC nodal voltage calculation. To assess the impact of variations in landing position on the measured S-parameters, the S-parameters of the probe were measured (as described in Section IV A) for various landing positions and landing angles. The studied positions were the center, top, bottom, left, and right of the calibration plate ports center conductor and the studied angles were -45, 0, and +45 degrees (along the dashed lines). These positions and angles are shown in Fig. 7.

For this sensitivity study, the 0-degree center S-parameter measurement was treated as the reference and all other S-parameter measurements were treated as measurements with some degree of variation in the landing position. The target IC nodal voltage was then calculated with (2) for three different target impedance cases: low, matched, and high (i.e. $Z_{\text{Target IC}}$ equal to 0.1 Ω , 50 Ω , and 1K Ω respectively), with B_2 equal to 1 (AC simulation). The maximum error observed over these landing variations was then calculated using (3) for each impedance case and is shown in Fig. 8.

$$Error (dB) = \max \left[dB \left(\frac{V_{Target \, Varration} (\omega)}{V_{Target \, Actual} (\omega)} \right) \right]$$
(3)

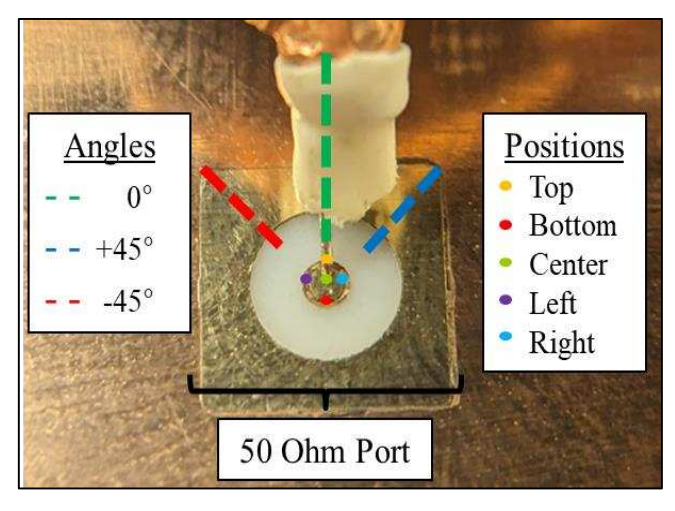


Fig. 7. Positions and angles used to test the impact of variation in landing position on S-parameter measurements. The measurement shown is in the 0-degree center position.

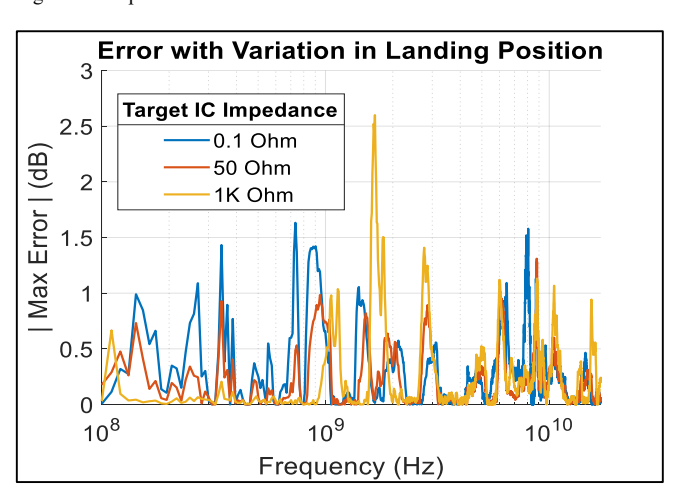


Fig. 8. The maximum error observed in the target IC waveform calculated among all the measured landing positions and various impedance conditions.

As shown in Fig. 8, the variations in landing position generally cause less than 2 dB of error in the calculation of the target voltage amplitude at the target IC during the injection. An exception to this observation is at 1.6 GHz for the high impedance case where 2.6 dB of error was observed. This case is an extreme example, however, and is unlikely to appear in practical measurements for the probe's usable range.

V. FEASIBILITY OF USING THE PROBE FOR RF INJECTIONS

To demonstrate the feasibility of using the probe experimentally, multiple injections were made into the 50 ohm loaded port of the characterization plate from section IV. This setup was used for simplicity because $\Gamma_{L3} = 0$.

Tests were performed using an Agilent M8190A Arbitrary Waveform Generator (AWG) as the source and an Agilent DSO81304B oscilloscope to record the waveforms at the IC node, port 3, and at the pickup port. A schematic and picture of the injection setup are shown in Fig. 9 and Fig. 10 respectively. All measurement cables, including the one

connected to the target port in the plate, were included in the calibration.

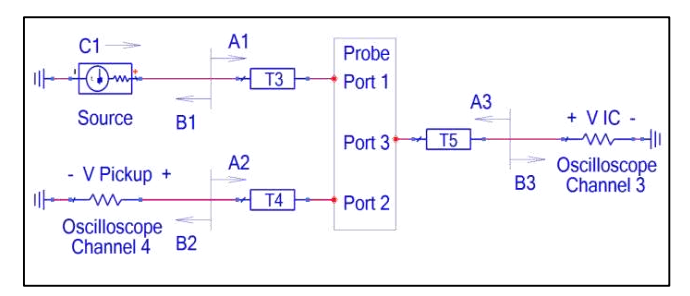


Fig. 9. Schmaic of the injection setup used to demonstrate the feasibility of the probe.

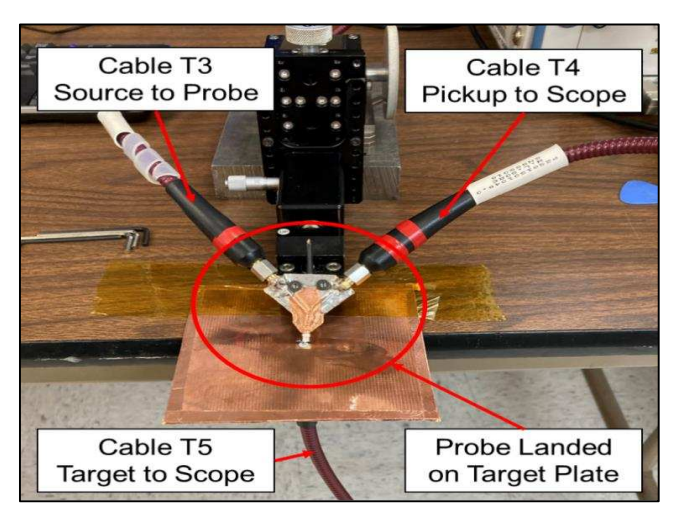


Fig. 10. The probe landed on the characterization plate from Section IV.

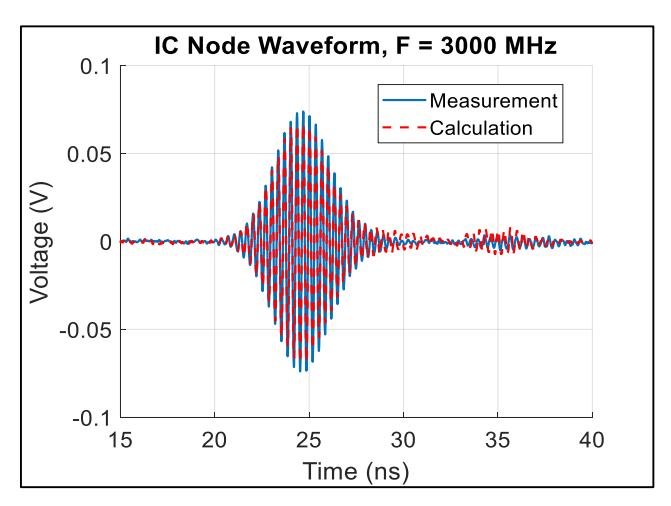


Fig. 11. Comparison between the measured waveform (blue) and the calculated waveform (red) for a 3000-MHz Gauss Sine 250.

Three waveforms were injected for validation: a 10 ns wide gated sinusoid (Sine10), a Gaussian modulated sinusoid with a 250-MHz bandwidth (Gauss Sine 250), and a damped sinusoid with a damping coefficient equal to 100E6 (Damped Sine 100). The injections were repeated for carrier frequencies from 500 to 5500 MHz at a 500 MHz step. The calculated

waveforms were then compared to the measured ones and the absolute error in the waveform at the IC pin was calculated as a difference in the peak values of the waveforms. Fig. 11 shows an example of this comparison for a 3000 MHz Gauss Sine 250 waveform. Fig. 12 shows the error over the entire test range for each test waveform.

Less than 2 dB of error was observed up to 5500 MHz with a peak error of 1.84 dB at 500 MHz. This error is comparable to the error estimates given in Section III.

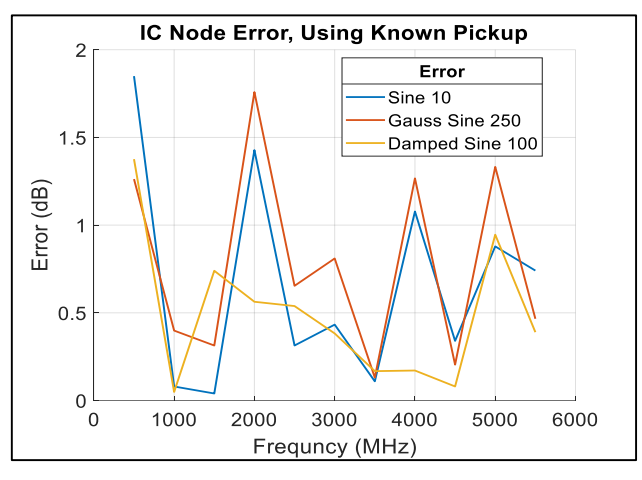


Fig. 12. Error in the peak value of the estimated waveform at the IC pin for the three test waveforms.

VI. DISCUSSION AND CONCLUSIONS

A direct injection probe with a capacitively coupled return and integrated voltage monitor was proposed in this work. As shown in Fig. 7, the probe is generally insensitive to variations in the landing position indicating that the S-parameters of the probe can be measured separately and used to estimate IC pin waveforms in later direct-injection measurements. During the S-parameter measurement, the authors noticed that the probe was sensitive to nearby objects (i.e., the hands of the authors). The authors suspect that this sensitivity is due to the stray common mode currents that run along the shield of the probe's coaxial cables. Adding ferrite absorbers to the probe plate and cables to suppress these stray currents has been proposed and is a topic of future work. Nevertheless, even without the common mode current suppressors the nodal voltage at the target IC can still be calculated with reasonable accuracy. While the results in Section V are not a complete validation, they do show the feasibility of the probe. Further validation of the probe is a topic of future work.

Overall, initial results demonstrate that the probe could be effective for in-system immunity characterization of ICs, where the IC cannot easily be placed on a separate, specialized test board. The probe allows one to measure the susceptibility of ICs embedded in complex systems while determining the waveform on-pin, and thus the IC's susceptibility on a pin-by-pin basis.

REFERENCES

 Integrated Circuits, Measurements of Electromagnetic Immunity 150 kHz to 1 GHz—Part 4: Direct RF Power Injection Method, Standard IEC 62132-4, 2006.

- [2] O. Aiello and P. Crovetti, "Characterization of the Susceptibility to EMI of a BMS IC for Electric Vehicles by Direct Power and Bulk Current Injection," in IEEE Letters on Electromagnetic Compatibility Practice and Applications, vol. 3, no. 3, pp. 101-107, Sept. 2021, doi: 10.1109/LEMCPA.2021.3085765.
- [3] S. Dai, X. Lu, Y. Zhang, L. Liu and W. Fang, "Electromagnetic Conductive Immunity of a Microcontroller by Direct Power Injection," 2021 6th International Conference on Integrated Circuits and Microsystems (ICICM), Nanjing, China, 2021, pp. 280-284, doi: 10.1109/ICICM54364.2021.9660326.
- [4] T. Sawada, K. Yoshikawa, H. Takata, K. Nii, and M. Nagata, "An Extended Direct Power Injection Method for In-Place Susceptibility Characterization of VLSI Circuits Against Electromagnetic Interference," in IEEE Transactions on Very Large Scale Integration (VLSI) Systems, vol. 23, no. 10, pp. 2347-2351, Oct. 2015, doi: 10.1109/TVLSI.2014.2361208.
- [5] T. Sawada, T. Toshikawa, K. Yoshikawa, H. Takata, K. Nii, and M. Nagata, "Evaluation of SRAM-core susceptibility against power supply voltage variation," IEICE Trans. Electron., vol. E95-C, no. 4, pp. 586–593, Apr. 2012.
- [6] T. Sawada, T. Toshikawa, K. Yoshikawa, H. Takata, K. Nii, and M. Nagata, "Immunity evaluation of SRAM core using DPI with on-chip diagnosis structures," in Proc. IEEE EMC Compo, Nov. 2011, pp. 65–70
- [7] J. Koo et al., "A Nonlinear Microcontroller Power Distribution Network Model for the Characterization of Immunity to Electrical Fast Transients," in IEEE Transactions on Electromagnetic Compatibility, vol. 51, no. 3, pp. 611-619, Aug. 2009, doi: 10.1109/TEMC.2009.2023670.
- [8] J. Zhang et al., "Modeling Injection of Electrical Fast Transients Into Power and IO Pins of ICs," in IEEE Transactions on Electromagnetic Compatibility, vol. 56, no. 6, pp. 1576-1584, Dec. 2014, doi: 10.1109/TEMC.2014.2332499.
- [9] Z. Peng et al., "Characterization and Modeling of Commercial ICs for System-Efficient ESD Design," in IEEE Transactions on Electromagnetic Compatibility, vol. 64, no. 6, pp. 1802-1811, Dec. 2022, doi: 10.1109/TEMC.2022.3217749.
- [10] Measuring and Modeling the Conducted Susceptibility of an Integrated Circuit Port to High-Frequency RF Waveforms (JDE)
- [11] G. Shen et al., "ESD Immunity Prediction of D Flip-Flop in the ISO 10605 Standard Using a Behavioral Modeling Methodology," in IEEE Transactions on Electromagnetic Compatibility, vol. 57, no. 4, pp. 651-659, Aug. 2015, doi: 10.1109/TEMC.2015.2418715
- [12] X. Wu, F. Grassi, G. Spadacini, S. A. Pignari, U. Paoletti and I. Hoda, "Investigation of Semi-Rigid Coaxial Test Probes as RF Injection Devices for Immunity Tests at PCB Level," in IEEE Access, vol. 8, pp. 147919-147929, 2020, doi: 10.1109/ACCESS.2020.3015282.
- [13] "Keysight Technologies Choosing the Best Passive and Active Oscilloscope Probes for Your Tasks." Available: https://www.keysight.com/us/en/assets/7018-03057/data-sheets/5990-8576.pdf
- [14] Keysight, "Technical Support: 85024A High-Frequency Probe, 300 kHz to 3 GHz," Keysight. https://www.keysight.com/us/en/support/85024A/high-frequency-probe-300-khz-3-ghz.html (accessed Jan. 03, 2024).
- [15] C. S. (Charles S. Lorens, "Theory and applications of flow graphs," dspace.mit.edu, 1956, Accessed: Jan. 07, 2024. [Online]. Available: https://dspace.mit.edu/handle/1721.1/4765.
- [16] "4.2: Measurement of Scattering Parameters," Engineering LibreTexts, Oct. 21, 2020. https://eng.libretexts.org/Bookshelves/Electrical_Engineering/Electronics/Microwave_and_RF_Design_III_-_Networks_(Steer)/04%3A_Chapter_4/4.02%3A_Section_2-(accessed Jan. 08, 2024).
- [17] Russer, Peter (2003). Electromagnetics, microwave circuit, and antenna design for communications engineering. Artech House. p. 420. ISBN 1-58053-532-1.